ACS OMEGA

Open Access

http://pubs.acs.org/journal/acsodf

Article

Loading Capsaicin onto Lipid Bilayers: A Molecular Dynamics Study

Nathanon Kerdkaen, Nililla Nisoh, Jiramate Kitjanon, Cristiano Dias, Mikko Karttunen, and Jirasak Wong-ekkabut*

Cite This: *ACS Omega* 2026, 11, 23728−23742

Read Online

ACCESS | Metrics & More | Article Recommendations | Supporting Information

ABSTRACT: Capsaicin is a natural bioactive compound found in chili peppers, with promising potential in various pharmacological applications, including analgesic, antipruritic, anti-inflammatory, anticancer, and antioxidant effects. Its clinical use, however, remains limited due to poor bioavailability, low aqueous solubility, and limited stability. To address these challenges, loading capsaicin in a small liposome bilayer has been proposed to enhance its transport across biological membranes. In this work, we perform molecular dynamics (MD) simulations to study the behavior of capsaicin in lipid bilayers. Two lipid types, 1-palmitoyl-2-oleoyl-*sn*-glycero-3-phosphocholine (POPC) and 1,2-dipalmitoyl-rac-*glycero*-3-phosphocholine (DPPC), are used to investigate the effects of unsaturation in the lipid tails. Simulations were conducted under two initial conditions: (1) capsaicin molecules placed in the aqueous phase to study permeation behavior and (2) capsaicin preinserted into the bilayer to assess its equilibrium positioning and to study its behavior in the membrane environment. Our results show that capsaicin tends to aggregate in water with only small aggregates capable of passive permeation into the membrane. The POPC bilayer exhibits a greater capsaicin uptake than the DPPC bilayer, which is attributed to its larger area per lipid. Mass-density profiles indicate the preferred localization of capsaicin within the bilayers, which is consistent with the minimum free energy observed in the potential of mean force (PMF) profiles for translocated molecules into the bilayer. Notably, capsaicin does not significantly change the bilayer thickness and area per lipid when the bilayer is in the liquid phase. It decreases the lipid area per lipid, while maintaining a stable area per capsaicin. The estimated area per capsaicin molecule within the bilayer is 0.415 ± 0.010 nm^2. Interestingly, when the bilayer was in the gel phase, the ordered lipid was disrupted by the capsaicin. These findings provide valuable insights into the membrane interactions of capsaicin and support the rational design of liposomal delivery systems to enhance its pharmaceutical potential.

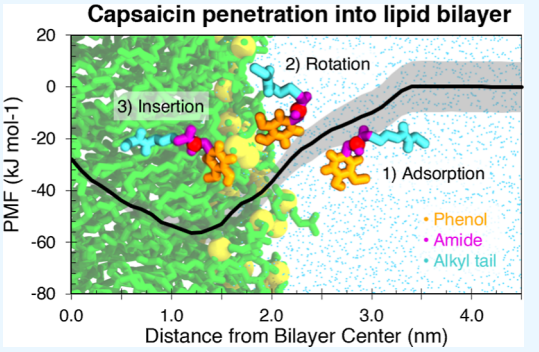

1. INTRODUCTION

Capsaicin (trans−8-methyl-*N*-vanillyl-6-nonenamide) is the active pungent compound found in chili peppers of the *Capsicum* genus. Capsaicin comprises a vanillyl group (containing a polar hydroxyl and methoxy group) linked via an amide bond to a hydrophobic alkyl chain. This dual polarity allows capsaicin to interact with both water and lipid environments. Capsaicin is widely recognized for its therapeutic potential, exhibiting a broad range of pharmacological activities, including analgesic, antipruritic, anti-inflammatory, anticancer, and antioxidant properties.[1−8] Its principal mechanism of action involves the activation of the transient receptor potential vanilloid type 1 (TRPV1) receptor, a nonselective cation channel expressed in nociceptive neurons, which plays a critical role in pain perception and thermoregulation.[9−12] Prolonged activation of TRPV1 by capsaicin leads to receptor desensitization, providing a basis for its analgesic effects.

Clinically, capsaicin has been incorporated into topical formulations, most notably in the form of an 8% dermal patch (Qutenza), which is FDA-approved for managing postherpetic neuralgia (PHN).[11,13−15] The Qutenza patch achieves therapeutic efficacy by inducing TRPV1 desensitization and the selective defunctionalization of nociceptive fibers. Lower concentration capsaicin creams (0.025%−0.075%) have also been used for other neuropathic pain conditions, such as diabetic neuropathy (DN), though clinical outcomes remain inconsistent and often inferior to first-line pharmacotherapies like gabapentinoids, tricyclic antidepressants, and serotonin−norepinephrine reuptake inhibitors.[16−20] Trials using the 8% capsaicin patch for diabetic peripheral neuropathy have yielded variable results, with side effects including transient burning and erythema, limiting routine clinical adoption.[18,21−23] Capsaicin has also been investigated for perioperative pain management due to its potential to reduce postoperative

Received: August 6, 2025
Revised: April 2, 2026
Accepted: April 3, 2026
Published: April 13, 2026

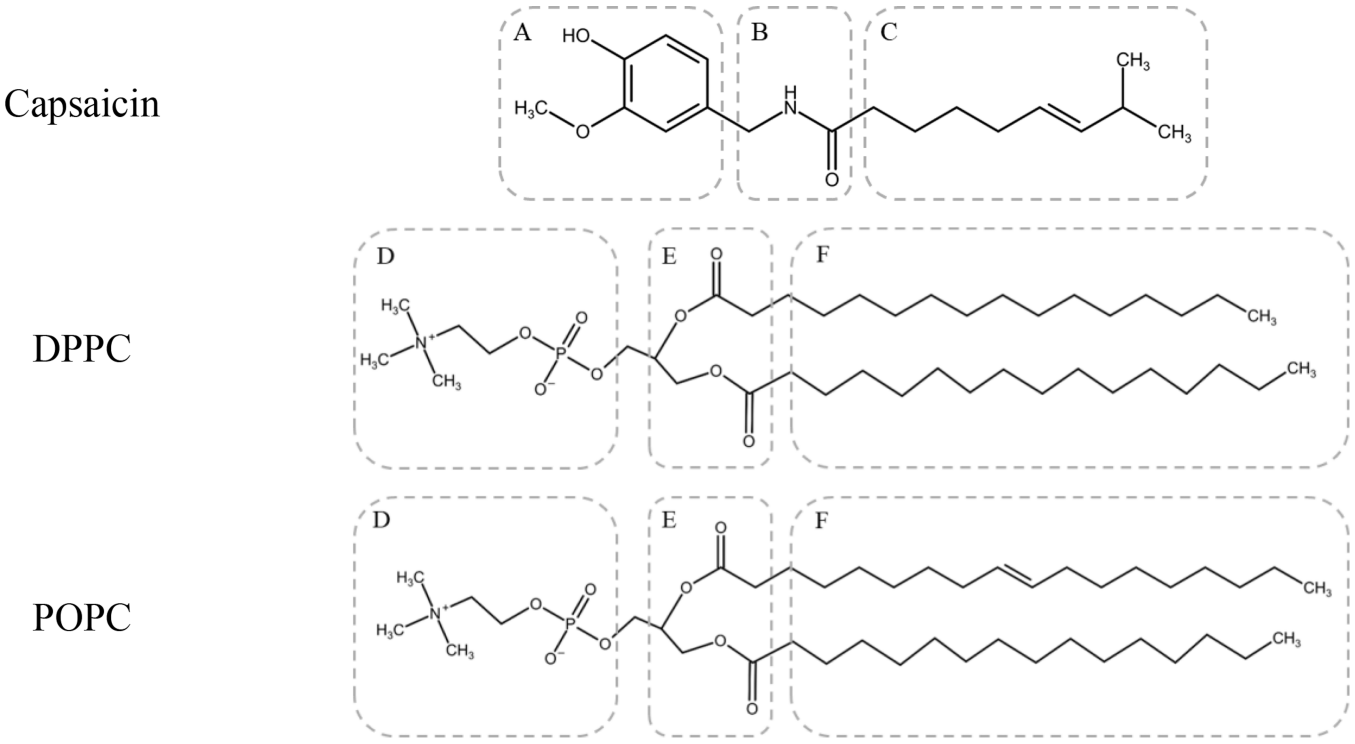

Figure 1. Chemical structures of capsaicin, DPPC, and POPC molecules. Regions of capsaicin molecules: (A) phenol group, (B) amide group, and (C) alkyl tail. Regions of lipid molecule: (D) choline group and phosphate group, (E) ester group, and (F) alkyl tail. The molecular parts are labeled according to their hydrophilic (A, B, D, E) and hydrophobic (C, F) properties.

analgesic requirements.[24−26] However, its clinical utility in this setting remains investigational, with ongoing trials being required to validate efficacy, optimize dosing regimens, and evaluate safety profiles. Capsaicin's clinical application is hampered by physicochemical limitations, including hydrophobicity, low aqueous solubility, chemical instability, and volatility, which restrict its bioavailability and cause dose-limiting adverse effects such as skin irritation and burning.[5,8,10,15,27] Various nanocarrier strategies have been explored to overcome capsaicin's physicochemical challenges.[5,7,8,10] Among these, liposomes offer unique advantages owing to their ability to encapsulate both hydrophilic and hydrophobic moieties within their bilayer structure, as well as their biocompatibility, potential for controlled release, and targeted delivery.[28−32] Phospholipids, such as dipalmitoylphosphatidylcholine (DPPC) and palmitoyl-oleoylphosphatidylcholine (POPC), are commonly employed in liposomal formulations for drug delivery.[31−33] Pharmacokinetic studies have demonstrated that capsaicin-loaded liposomes can reduce mucosal irritation and enhance bioavailability.[34] Moreover, encapsulation in the liposomal bilayer has been shown to prolong drug release and increase cytotoxic selectivity in cancer models.[35,36]

Previous experimental studies[37−40] using nuclear magnetic resonance (NMR), X-ray diffraction, fluorescence spectroscopy, and differential scanning calorimetry (DSC) have elucidated that capsaicin preferentially localizes at the lipid−water interface, with its vanillyl (phenolic) headgroup anchoring in the headgroup/carbonyl region, and the hydrophobic tail penetrating the upper acyl chain core. These studies also indicate that capsaicin generally fluidizes membranes by lowering the phase transition temperatures, though concentration- and composition-dependent rigidifying effects have also been observed in cholesterol-containing systems.[41−44]

Although experimental techniques can provide structural information, they are often insufficient to resolve transient and dynamic interactions at the molecular level. In this regard, molecular dynamics (MD) simulations serve as a powerful tool to study the physicochemical behavior of drugs within lipid bilayers. Previous MD studies have successfully characterized the partitioning, orientation, and permeation of various small molecules and peptides in membrane systems.[45−54] MD simulation studies show the favorable interfacial partitioning of the capsaicin molecule with free energy minima in the lipid bilayer and significant translocation of energy barrier between leaflets.[55−58] MD simulations have extensively characterized the interaction of capsaicin with the lipid bilayer, revealing its role as a membrane modifier and a specific ligand. Early computational studies established the amphiphilic nature of capsaicin, showing that it preferentially partitions into the membrane interface where its vanillyl headgroup forms hydrogen bonds with lipid carbonyls and the hydrophobic tail penetrates the bilayer core.[55,59] This interfacial accumulation changes bulk membrane properties, thinning bilayer, and increased elasticity resulting in the nonspecifically modulated functions of membrane proteins.[57,60] Furthermore, recent advanced sampling techniques have elucidated the specific access mechanism of capsaicin to the intracellular binding site of the TRPV1 channel. A membrane-mediated pathway demonstrated that the ligand undergoes a "flip-flop" or direct entry from the lipid phase to the TRPV1 binding pocket.[55,58]

Despite extensive experimental and computational studies, the molecular-level mechanisms governing capsaicin insertion, preferred orientation, and its influence on the lipid phase remain incompletely understood. In particular, how capsaicin's amphiphilic structure drives its interfacial localization, hydrogen-bonding interactions with lipid headgroups, and concen-

https://doi.org/10.1021/acsomega.5c07901
ACS Omega 2026, 11, 23728−23742

Table 1. The Simulation Systems

no	systems	lipid type	capsaicin/lipid ratios	number of molecules in systems			simulation time (ns)
				#Capsaicin	#Lipid	#Water	
1	Adding capsaicin in water phase	DPPC	-	1	128	11,705	200
2		POPC	-	1	128	11,705	200
3		DPPC	-	3	128	11,705	300
4		POPC	-	3	128	11,705	300
5		DPPC	-	5	128	11,705	500
6		POPC	-	5	128	11,705	500
7		DPPC	-	10	128	11,705	500
8		POPC	-	10	128	11,705	500
9	Inserting capsaicin inside lipid bilayer	DPPC	0.00	0	512	25,600	500
10		POPC	0.00	0	512	25,600	500
11		DPPC	0.10	56	512	26,128	500
12		POPC	0.10	56	512	26,128	500
13		DPPC	0.20	104	512	25,872	500
14		POPC	0.20	104	512	25,872	500
15		DPPC	0.30	152	512	25,896	500
16		POPC	0.30	152	512	25,896	500
17		DPPC	0.40	208	512	25,920	500
18		POPC	0.40	208	512	25,920	500
19		DPPC	0.50	256	512	26,112	500
20		POPC	0.50	256	512	26,112	500
21	Constraint	POPC	-	1	128	13,988	300
22		DPPC	-	1	128	10,367	300

tration-dependent effects on bilayer physical properties is still unresolved. In this study, we employ extensive MD simulations to investigate capsaicin's behavior in dipalmitoylphosphatidylcholine (DPPC) and palmitoyl-oleoylphosphatidylcholine (POPC) bilayers. We analyze capsaicin's preferred location, orientation, interaction energies, and influence on the bilayer structure, including area per lipid, volume per lipid, bilayer thickness, deuterium order parameters, and water permeability. Our findings provide molecular-level insights into capsaicin–lipid interactions, supporting the rational design of capsaicin-loaded liposomal formulations with improved therapeutic performance, guiding both experimental formulation strategies and potential clinical applications.

2. METHODOLOGY

2.1. Molecular Dynamics (MD) Simulations

Atomistic MD simulations were performed to study the permeation behavior of capsaicin across lipid bilayers and to assess its effects on the membrane structure. Two types of phospholipid bilayers were used: DPPC to represent saturated lipids and POPC to represent unsaturated lipids. The force field parameters for both lipids and capsaicin were taken from the GROMOS 54a7 united-atom force field.[61−65] Molecular structures for DPPC and POPC were obtained from previous studies,[52,66] and capsaicin topologies were generated using the Automated Topology Builder (ATB).[64,65] The chemical structures of capsaicin and lipids are shown in Figure 1.

Initial bilayer configurations were generated using the MemGen online membrane builder,[67] and bilayers were fully hydrated with simple point charge (SPC) water molecules.[68] Two simulation setups were employed: (1) Capsaicin permeation studies: A single capsaicin molecule and clusters of 3, 5, or 10 molecules were randomly placed in the aqueous phase, 2.0 nm away from the lipid–water interface. Each bilayer consisted of 128 lipid molecules (64 per leaflet). These simulations were designed to examine the permeation process of capsaicin, following protocols commonly used in membrane transport studies.[43,69,70] (2) Capsaicin–bilayer interaction studies: Larger bilayers composed of 512 lipid molecules (256 per leaflet) were used to study the impact of capsaicin on the bilayer properties. Capsaicin molecules were directly embedded in the membrane with a uniform distribution. In the initial configuration, they were positioned at the bilayer interface with the polar phenol group oriented toward the lipid phosphate region and the alkyl tail extending toward the bilayer core, consistent with the preferred insertion observed in the capsaicin permeation studies. The number of added capsaicin molecules was varied, 0, 56, 104, 152, 208, and 256 molecules, corresponding to capsaicin/lipid molar ratios of 0.00, 0.10, 0.20, 0.30, 0.40, and 0.50, respectively. Detailed system parameters are listed in Table 1.

All systems underwent energy minimization using the steepest descent algorithm to remove steric clashes and voids. Subsequently, the production MD simulations were carried out for 500 ns with a 2 fs time step using GROMACS version 2022.6.[71,72] Simulations were conducted in the isothermal–isobaric (*NPT*) ensemble. Pressure was maintained at 1.0 bar using a semi-isotropic Parrinello–Rahman barostat[73] with a time constant of 3.0 ps and compressibility of 4.5×10^{-5} bar^{-1}. Temperature was controlled at 310 K using the velocity-rescaling thermostat with a time constant of 0.1 ps.[74] Periodic boundary conditions were applied in all directions. The neighbor list was updated at every step. A cutoff of 1.0 nm was applied for the van der Waals and real-space parts of electrostatic interactions. Long-range electrostatics were calculated using the smooth Particle Mesh Ewald (SPME) method,[75−77] with reciprocal–space interactions computed on a 0.12 nm grid using fourth-order cubic interpolation. The Lennard-Jones potentials were shifted to zero at 1.0 nm by using a potential-shift modifier. All bond lengths were constrained using the *P*-LINCS algorithm.[78] A

https://doi.org/10.1021/acsomega.5c07901
ACS Omega 2026, 11, 23728−23742

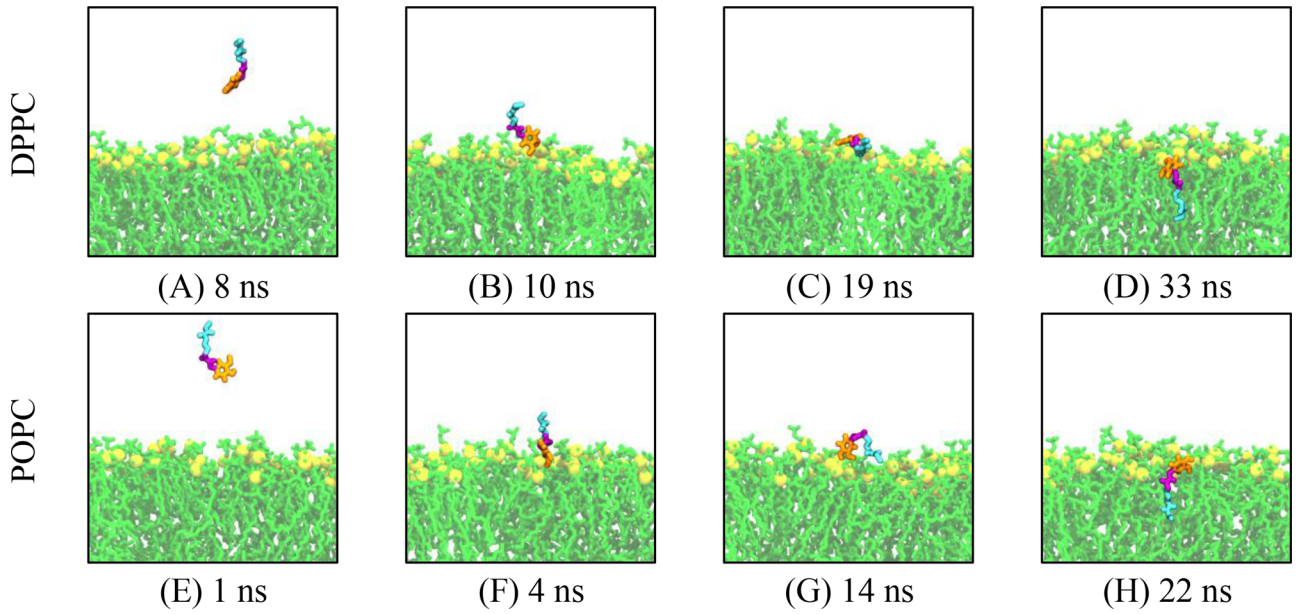

Figure 2. Side-view snapshots from atomistic MD simulations illustrate the translocation pathway of a single capsaicin molecule from the aqueous phase into the (A−D) DPPC and (E−H) POPC lipid bilayer. The selected snapshots represent the key stages of capsaicin insertion. The phenol group, amide group, and carbon tail of capsaicin are represented in orange, purple, and light blue, respectively. Lipids are depicted in green, with phosphate groups highlighted as yellow spheres. Water molecules are not shown for ease of observing capsaicin molecules.

trajectory visualization was performed using Visual Molecular Dynamics (VMD).[79] The temperature of 310 K was selected to mimic human body temperature, despite being slightly below the phase transition temperature of DPPC (313 K). This temperature was still suitable for our study as we carefully assessed the phase state of the lipid bilayers using the visualization and order parameter, which confirmed that both DPPC and POPC were in the disordered phase at this temperature. In addition, the optimized parameters and protocols have been extensively tested and used previously, in refs 52,80−82. The area per lipid (APL), bilayer thickness, and volume per lipid (VPL) were analyzed as the fundamental parameters for characterizing the structural properties of the bilayers. In this study, these parameters were systematically analyzed based on the Voronoi tessellation via the APL@Voro software.[83,84] APL@Voro computes individual Voronoi areas for each lipid and capsaicin molecule, enabling independent reporting of the area per molecule for both components independently. Tessellation was performed using the hydroxy oxygen of the capsaicin phenol group and the phosphate atom of the lipid headgroup as reference points, both projected onto the bilayer plane. The bilayer thickness was determined by averaging the distances between the local centers of mass (COMs) of the lipid phosphate group in opposing leaflets. Volume per lipid was then obtained by multiplying the APL by half the bilayer thickness. The order parameters of the lipid tails were computed by the gorder[85] tool, which reconstructs C−H bond vectors from united-atom models for accurate analysis. Finally, the number of water permeation events was analyzed using in-house Python scripts[86] based on NumPy[87] and MDAnalysis libraries.[88,89]

2.2. Constraint Simulations for Free Energy Calculation

Constraint-based MD simulations were conducted to compute the free energy profile associated with the translocation of a capsaicin molecule from the water phase into the DPPC and POPC lipid bilayers. A total of 46 independent simulations were performed, in which the distance between the COM of the capsaicin molecule and that of the bilayer were restrained at discrete intervals ranging from 0 to 4.5 nm, with a spacing of 0.1 nm. A harmonic constraint with a force constant of 1000 kJ mol^{-1} nm^{-2} was applied, with a relative tolerance set to 10^{-6}. Each system comprised 128 lipid molecules and was solvated with SPC water. Simulations were conducted under the *NPT* ensemble at 298 K. Each window was simulated for 300 ns to ensure convergence.

The free energy profile, $\Delta G(z)$, describing the transfer of capsaicin from the water phase into the lipid bilayer, was computed via numerical integration of the average constraint force, $\langle F(z')\rangle_t$, over the translocation pathway

$$\Delta G(z) = -\int_{\text{water phase}(z=4.5\,nm)}^{z} \langle F(z')\rangle_t dz' \quad (1)$$

here, $\langle F(z')\rangle_t$ denotes the mean force acting on the capsaicin molecule at a specific position z' along the bilayer normal. The integration proceeds from the bulk water region (z = 4.5 nm) toward the interior of the membrane.

To assess the statistical uncertainty in the computed forces, block averaging was employed using the final 30 ns of each trajectory divided into ten equal segments. This methodology ensures robust estimation of the free energy landscape, as previously demonstrated in similar bilayer permeation studies.[90,91]

3. RESULTS AND DISCUSSION

3.1. Attraction and Adsorption of Capsaicin Molecules into Lipid Bilayers

Capsaicin is an amphiphilic molecule consisting of both hydrophilic moieties (phenol group and amide group) and hydrophobic (alkyl tail) moieties. The chemical structure of capsaicin is shown in Figure 1. Experimental studies have shown that it strongly prefers to embed itself in a lipid environment instead of remaining solvated.[92−95] This is

https://doi.org/10.1021/acsomega.5c07901
ACS Omega 2026, 11, 23728−23742

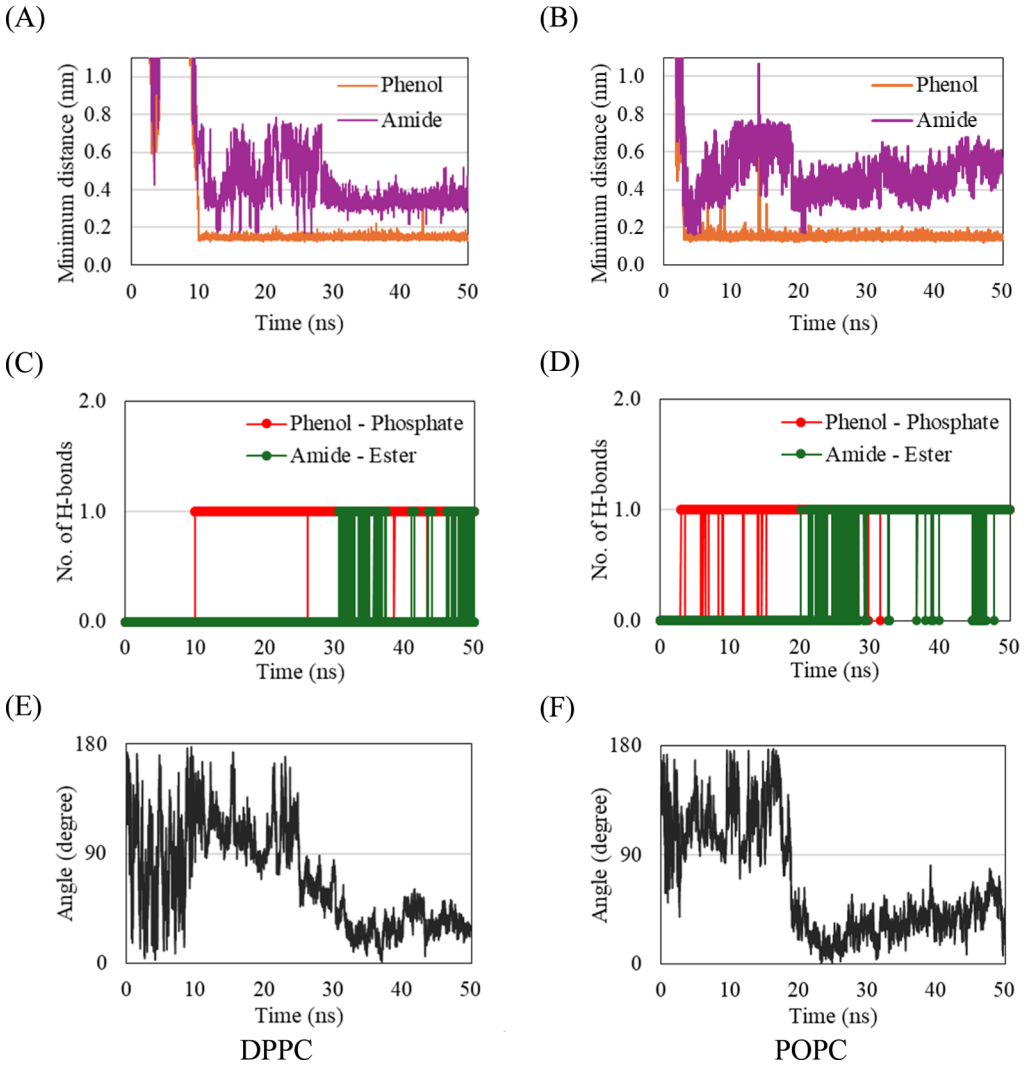

Figure 3. Analysis of capsaicin insertion dynamics in DPPC and POPC bilayers from single-capsaicin simulations. (A,B) Minimum atomic distances between the phenol and amide groups of capsaicin and the phosphate groups of lipids. (C,D) Number of hydrogen bonds formed between the capsaicin phenol group and lipid phosphate groups and between the capsaicin amide group and lipid ester groups. (E,F) Orientation angle of capsaicin relative to the bilayer normal, defined as the angle between the vector connecting hydroxyl oxygen of phenol group and terminal tail methyl carbon and the bilayer normal (*z*-axis). Only the first 50 ns of the 200 ns trajectories are shown, as the relevant interactions occur within this time window and remain stable afterward.

consistent with results from our simulations, in which capsaicin molecules are initially introduced in the water phase. In these simulations, capsaicin is promptly attracted to the polar headgroup regions of the DPPC (saturated) and POPC (monounsaturated) lipids. This is illustrated in Figure 2, which shows the phenolic moiety of capsaicin (highlighted in orange) being driven to the water−lipid interface (Figure 2A,B). Following this initial contact, the hydrophobic tail of capsaicin, which remained exposed to water, undergoes a rotation (flip) to allow its insertion into the hydrophobic core of the bilayer (Figure 2C). Once inserted, capsaicin adopts a stable configuration, with the phenolic head located near the lipid−water interface and the hydrophobic tail aligned approximately parallel to the bilayer normal (Figure 2D). The snapshots of initial and final configurations are shown in Figure S1. This membrane-anchored configuration is energetically favorable and has been consistently observed in simulations using different force fields.[55]

The insertion of capsaicin is quantified in Figure 3 where (i) the minimum atomic distance and (ii) the number of hydrogen bonds between capsaicin and the lipids are shown as well as (iii) the angle of capsaicin relative to the bilayer normal. The partial simulation time in Figure 3 is chosen to capture the events of interest, and the complete 200 ns time evolution of capsaicin insertion dynamics is shown in Figure S2.

Figure 3A,B compares the minimum distance of lipid phosphate groups to phenol (orange line) and amide (purple line) moieties of capsaicin for DPPC and POPC bilayers. The minimum atomic distance between the capsaicin phenol group and the lipid phosphate group rapidly decreased and stabilized at approximately 0.15 nm within the first 3 and 10 ns of the simulations for POPC and DPPC, respectively. The distance remained stable throughout the remainder of the simulations. Although the minimum atomic distances between the capsaicin amide group and the lipid phosphate group also decreased following phenol insertion, they stabilized around 0.5 nm. These observations indicate that, upon approaching the

https://doi.org/10.1021/acsomega.5c07901
ACS Omega 2026, 11, 23728−23742

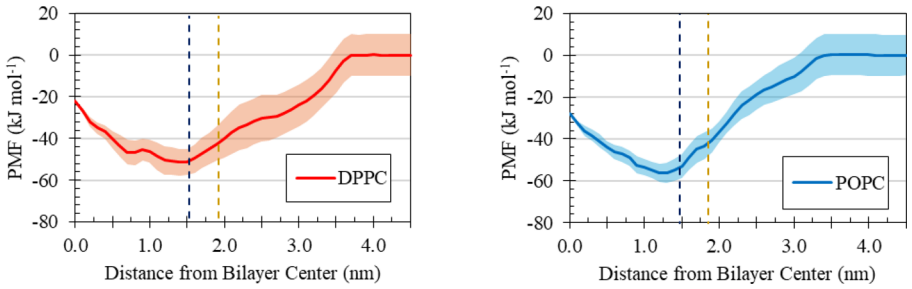

Figure 4. Potential of the mean force (PMF) profiles for the translocation of a capsaicin molecule into DPPC and POPC bilayers. The profiles were obtained using a biased simulation, in which capsaicin was moved from the water phase (4.5 nm) to the bilayer midplane (0.0 nm) along the bilayer normal. The free energy in the water phase was set to zero. Vertical dot-dashed yellow and blue lines indicate the positions of lipid phosphate and ester groups, respectively.

bilayer, capsaicin adopts orientations driven by hydrophilic and hydrophobic interactions. The more rapid insertion of phenol groups onto the lipid headgroups in POPC compared to the DPPC bilayers may be attributed to the higher area per lipid (APL) of the former membrane. Consistent with other studies,[41,96−99] the APLs of the POPC and DPPC bilayers in our simulations are 0.652 ± 0.002 nm^2 and 0.625 ± 0.003 nm^2, respectively. This greater lateral spacing between lipid molecules in POPC results in a less tightly packed environment within headgroups, enabling a more prompt insertion of the phenol group.

The presence of a hydrogen donor atom at the phenol moiety of capsaicin as well as hydrogen acceptor atoms at the phosphate groups of DPPC and POPC lipids (Figure 1) suggests that the strong interaction between these groups could originate from hydrogen bonding. To quantify this, hydrogen bonds were defined using the standard geometric criteria[100−102] of a donor−acceptor distance closer than 0.35 nm and a donor−hydrogen−acceptor angle in a range of 150°−180°. The interaction between capsaicin and lipid is confirmed in Figure 3C,D, which shows one stable hydrogen bond forming between the capsaicin phenol and the lipid phosphate group (red lines) as soon as their distance becomes minimal, as seen in Figure 3A,B at 10 ns for DPPC and at 3 ns for POPC. Figure 3C,D also shows one hydrogen bond forming between the amine group of capsaicin and the carbonyl oxygen in the ester group of the DPPC and POPC lipids. The latter takes place after phenol insertion, and it is only possible after the hydrophobic tail of capsaicin penetrates the bilayer core. This is confirmed in Figure 3E,F, which measure the angle between a vector connecting the hydroxyl oxygen of the phenol group and the terminal methyl carbon of the hydrocarbon tail relative to the bilayer normal (z-axis). Before the insertion of the phenol group (0−10 and 0−3 ns for DPPC and POPC, respectively), the capsaicin tail adopts a mostly random orientation. After insertion (30−50 and 20−50 ns for DPPC and POPC, respectively), it adopts mostly angles that are larger than 90°, which is a characteristic of configurations where the capsaicin tail sticks out of the lipid head groups. The slower rotation of the capsaicin tail in DPPC compared to the POPC bilayers supports the notion that membrane compactness slows capsaicin dynamics. Notice that the full insertion of capsaicin also coincides with the formation of hydrogen bonds between its amine group and the ester group in Figure 3E,F. This highlights the importance of hydrogen bonding in both holding the phenol group at the water−lipid interface and in accounting for the orientation of the capsaicin tail in the dry core of the bilayer.

3.2. Transferring a Capsaicin Molecule from Water to the Lipid Bilayer

Here, we compute the potential of mean force (PMF) to insert capsaicin into lipid bilayers in order to provide insights into its preferred location inside the membrane. The PMF is computed using umbrella sampling simulations[103,104] and using the distance ξ between the center of mass of capsaicin, and the bilayer center as a reaction coordinate. For convenience, the PMF when capsaicin is in bulk water (i.e., ξ > 3.5 nm) is used as our reference. Figure 4 shows the PMF profiles in simulations using DPPC and POPC membranes revealing distinct minima at approximately 1.4 and 1.2 nm from the bilayer center, respectively, which coincide approximately with the lipid ester group (vertical blue dashed lines). The PMFs to transfer capsaicin from bulk water to these preferred locations in the membrane are −51.34 ± 5.42 kJ/mol and −56.32 ± 4.67 kJ/mol for DPPC and POPC, respectively. These low PMF values indicate strong binding to the lipid bilayer. Interestingly, the insertion of capsaicin into the bilayer is not characterized by any visible energy barrier suggesting that capsaicin makes its way through the water−lipid interface spontaneously without facing significant steric constraints. Moreover, the energy barrier to flip capsaicin from one of the bilayer leaflets to the other is given by computing the difference in the PMF at the bilayer center (ξ = 0) and at its minimum (ξ = 1.4 or 1.2 nm). For our simulations performed using DPPC and POPC, the energy barriers are 29.28 ± 2.07 kJ/mol and 28.50 ± 1.46 kJ/mol, respectively. These energy barriers are more than an order of magnitude greater than the thermal energy (2.47 kJ/mol), indicating that spontaneous translocation is highly improbable in atomistic simulations. Thus, migration through the bilayer midplane can be considered a rare and energetically costly event for capsaicin in phospholipid bilayers.

Our findings are consistent with previous studies employing OPLS and CHARMM36 force fields, which reported comparable PMF profiles for capsaicin insertion and leaflet transition.[55,58] While methodological differences may account for variations in reported barrier heights, previously published values for capsaicin insertion into the POPC range from 48.12 kJ/mol (OPLS) to 20.92 kJ/mol (CHARMM36). It is worth noting that Hanson et al.[55] observed one instance of capsaicin translocating between POPC leaflets in their simulations. However, no such flip-flop events were recorded in our simulations, further reinforcing that interleaflet migration is a rare and energetically costly event for capsaicin in phospholipid bilayers.

https://doi.org/10.1021/acsomega.5c07901
ACS Omega 2026, 11, 23728−23742

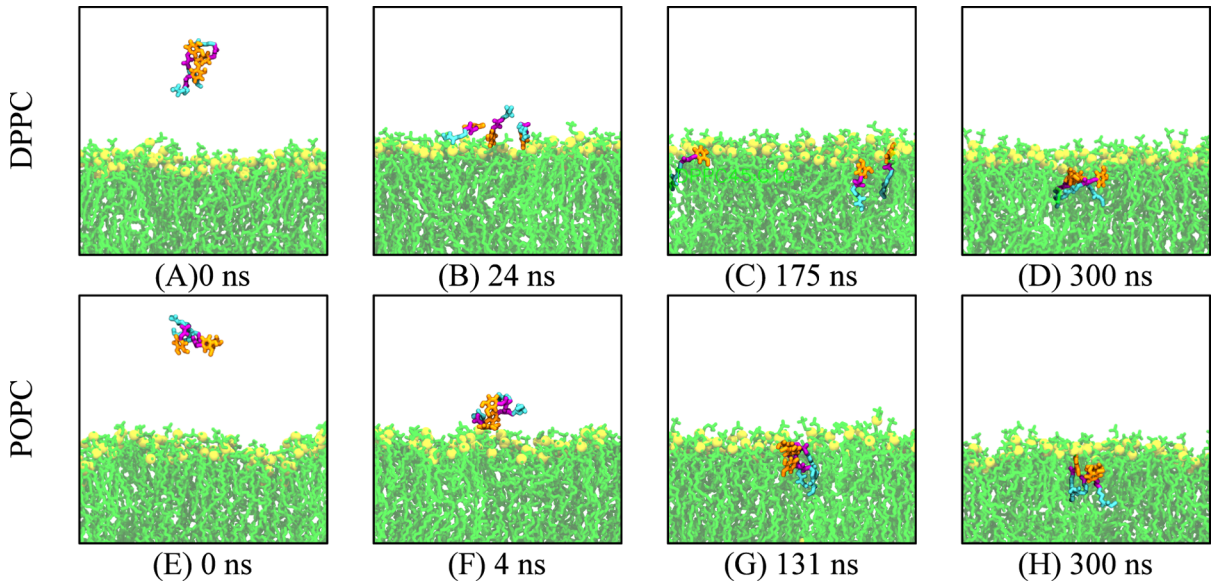

Figure 5. Side-view snapshots from atomistic MD simulations showing the insertion process of a three-capsaicin cluster into the DPPC (A-D) and POPC (E-H) bilayers. The selected snapshots illustrate the key stages of cluster adsorption. Lipid molecules are depicted in green, with phosphate groups highlighted as yellow spheres. Capsaicin molecules are color-coded by functional groups: phenol in orange, amide in purple, and alkyl tail in light blue. Water molecules are omitted for clarity.

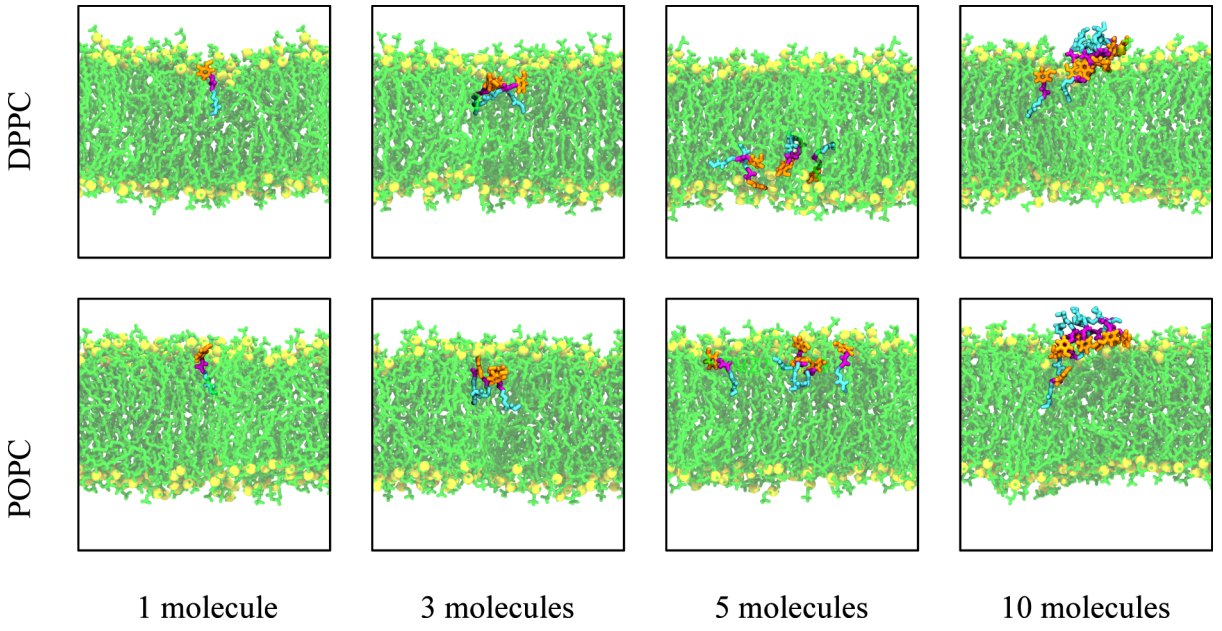

Figure 6. Side-view snapshots of bilayer configurations at the end of simulations with 1, 3, 5, and 10 capsaicin molecules with the DPPC and POPC bilayers. Lipid molecules are depicted in green, with phosphate groups highlighted as yellow spheres. Capsaicin molecules are color-coded by functional groups: phenol in orange, amide in purple, and alkyl tail in light blue. Water molecules are omitted for clarity.

3.3. Impact of Capsaicin Aggregation on Membrane Insertion

Due to their amphiphilic nature, capsaicin tends to aggregate in solution. Since membrane insertion of individual capsaicin molecules and aggregates may differ, additional simulations were performed with 3 molecules initially placed in the water phase. In these simulations, capsaicin molecules cluster before they insert into the bilayer. Figure 5 shows the time evolution of the membrane structure throughout the simulation. The insertion starts with the phenol moieties of the capsaicin aggregates interacting with lipid head groups, followed by the rotation of the hydrophobic tail of capsaicin leading to its full insertion into the membrane. The rotation of the capsaicin's tails is faster in POPC (~131 ns) compared to DPPC (~175 ns), consistent with POPC's lower lipid packing density (higher APL) that accounts for a smaller energetic and steric barrier of insertion. Moreover, the time scales to induce capsaicin tail rotation in simulations made with three molecules (~130−180 ns) are significantly larger than in simulations performed with a single molecule (~20−30 ns), as illustrated in Figure 3E,F. This can be rationalized by the more challenging passage of capsaicin's tails in large clusters through lipid headgroups as compared to the equivalent passage in small aggregates due to increased steric repulsion with lipid

https://doi.org/10.1021/acsomega.5c07901
ACS Omega 2026, 11, 23728−23742

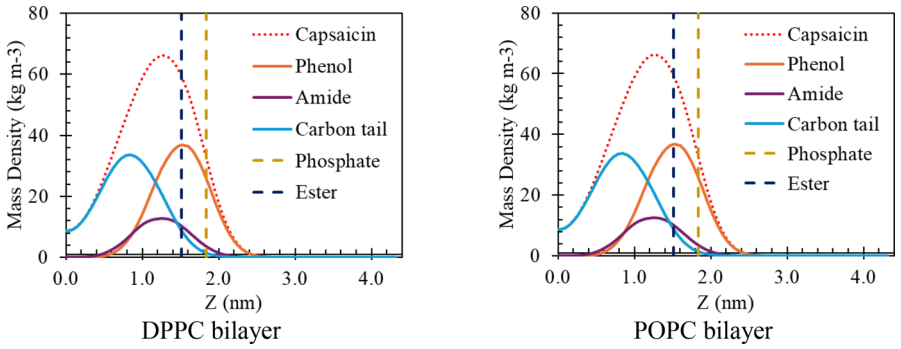

Figure 7. Mass-density profiles of capsaicin along the bilayer normal for DPPC and POPC bilayers. Profiles are averaged over both leaflets and shown for one leaflet for clarity. Vertical dot-dashed lines mark the positions of lipid phosphate and ester groups at ∼1.85 and ∼1.50 nm from the bilayer center, respectively. Results are shown for a representative system with a 0.10 capsaicin-to-lipid ratio; similar distributions were observed across all capsaicin-to-lipid ratios.

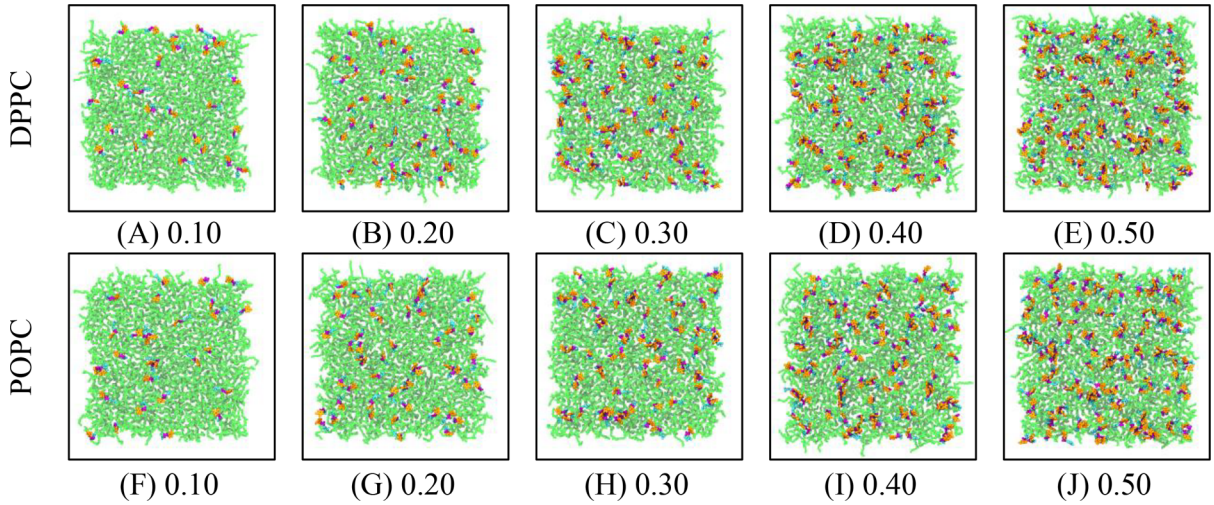

Figure 8. Top-view snapshots of embedded capsaicin in the (A−E) DPPC and (F−J) POPC bilayers at the end of the 500 ns simulations at different capsaicin-to-lipid ratios. Lipids are shown in green. Capsaicin molecules are distinguished by functional groups: phenol (orange), amide (purple), and alkyl tail (light blue). For clarity, only the upper leaflet is displayed, and water molecules are omitted.

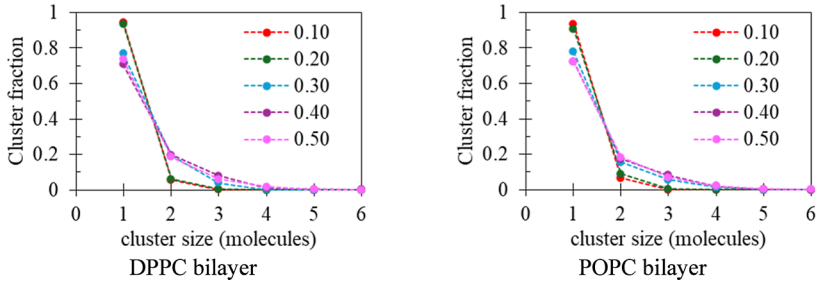

Figure 9. Cluster fraction of capsaicin molecules within the DPPC and POPC lipid bilayers. Different colors correspond to varying capsaicin-to-lipid ratios. A clustering cutoff of 0.23 nm was applied, defined by the first minimum of the radial distribution function (RDF) between capsaicin atoms.

headgroups. Moreover, this is also consistent with the results from additional simulations of 3 capsaicin molecules performed for 300 ns and 5 and 10 capsaicin molecules performed for 500 ns simulation. The last configuration of these simulations is shown in Figure 6. It shows that only the systems containing 10 capsaicin molecules form large surface-bound clusters that persisted at the interface after 500 ns in both DPPC and POPC bilayers. Interestingly, only a limited number of molecules from large clusters can penetrate the membrane, suggesting that aggregation reduces the efficiency of bilayer permeation.

3.4. Interaction of Capsaicin within the Bilayer and Local Structure Perturbations

At low concentrations, capsaicin molecules may individually insert themselves into the membrane and aggregate subsequently. To examine this pathway, simulations with 52 capsaicin molecules inserted into DPPC and POPC bilayers containing 512 lipid molecules were studied. In Figure 7, we investigated the mass−density profiles of phenol, amide, and

https://doi.org/10.1021/acsomega.5c07901
ACS Omega 2026, 11, 23728−23742

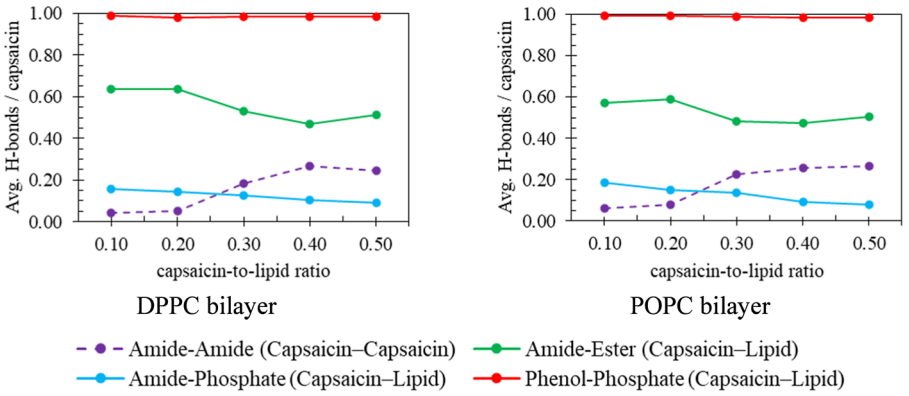

Figure 10. Average number of hydrogen bonds formed per capsaicin molecule in the concentration-dependent simulations of DPPC and POPC bilayers. Each line represents hydrogen bonding between specific capsaicin functional groups and either lipid groups or other capsaicin molecules. The *y*-axis label "Avg. H-bonds/capsaicin" refers to the average number of hydrogen bonds per capsaicin molecule.

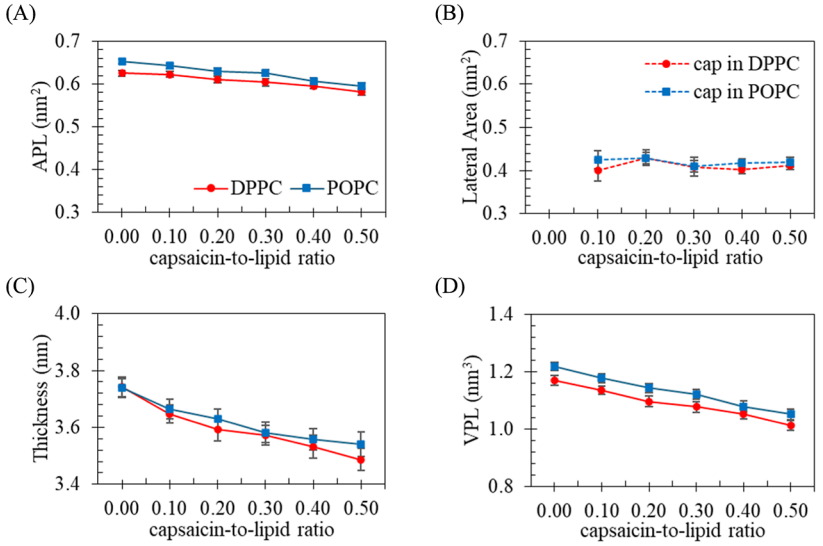

Figure 11. Structural properties of the DPPC (red) and POPC (blue) bilayers as a function of the capsaicin-to-lipid ratio. (A) Area per lipid (APL), (B) lateral area per capsaicin molecule, (C) bilayer thickness, and (D) volume per lipid (VPL). Solid lines represent values calculated for the lipid molecules, while the dotted lines indicate values associated with capsaicin molecules.

hydrophobic tail regions of capsaicin relative to those of the bilayer center. The phenol group (orange line) aligns closely with the ester group region of the lipids (vertical dashed blue line), supporting the PMF results that capsaicin prefers the interfacial region near lipid headgroups. This distribution is also consistent with previous works by Swain et al.[37] and Domene et al.[58] The capsaicin amide group (purple line) lies between their phenol group and carbon tail, consistent with their structure that the amide group links polar phenol to the nonpolar alkyl tail. The mass−density profile of the hydrocarbon tail of capsaicin (light blue line) is more broadly distributed, extending from the phosphate headgroups toward the bilayer's center. The broad distribution of capsaicin's tail is the result of conformational flexibility and weak interaction with the lipid tails. Accordingly, capsaicin adopts an amphiphilic orientation, with its phenol group located at the polar interface and its tail penetrating the hydrophobic region of the bilayer. This enables capsaicin to maintain a dynamic but stable embedding within the membrane. No significant spatial differences were noted between DPPC and POPC systems, in accordance with the minimal variation in the PMF minima between the two lipid types. To investigate the effects of capsaicin on the properties of the bilayer, simulations were performed by varying the concentration of capsaicin molecules in the membrane, i.e., capsaicin-to-lipid ratios from 0.00 to 0.50. Snapshots of the last frame of the simulations (Figure 8) show that capsaicin largely dispersed in the membrane. The cluster analysis in Figure 9 shows that over 90% of capsaicin molecules exist as monomers and only small fractions of dimer and trimer are found at high capsaicin concentrations. Interestingly, the hydrogen bond analysis (Figure 10) reveals that the phenol moieties of capsaicin extensively form hydrogen bonds with lipid phosphate groups (red lines). The dominance of hydrogen bond between capsaicin−lipid molecules suggests a strong affinity of capsaicin to the membrane.

The lateral area per capsaicin was calculated using the APL@Voro method. For capsaicin embedded in the DPPC and POPC bilayers, the lateral area is 0.415 ± 0.010 nm^2. These values remained consistent across all concentrations, indicating a stable interfacial accommodation of capsaicin within the membrane. In addition, bioactive molecules like cholesterol, curcumin, and α-tocopherol (vitamin E) are known to influence the lipid membrane structure. Cholesterol

https://doi.org/10.1021/acsomega.5c07901
ACS Omega 2026, 11, 23728−23742

inserts deeply into the membrane, increasing tail order and bilayer thickness.[41,42,53,105] Curcumin, with its planar amphiphilic structure, disrupts lipid packing by deep insertion and multiple hydrogen bonds with lipids.[106−108] In contrast, α-tocopherol anchors primarily at the lipid−water interface via its polar headgroup and passively penetrates into the bilayer. Interestingly, the α-tocopherol flip-flop between bilayer leaflets has been observed, an important function to help stabilize the membrane structure under oxidative stress.[46,48,109,110]

To investigate the effects of capsaicin on the membrane structure, Figure 11 shows the area per lipid (APL), the bilayer thickness, and volume per lipid (VPL) at different capsaicin/lipid ratios. The APL of the lipid was also calculated using the APL@Voro method. Pure DPPC and POPC membranes have APLs of 0.625 ± 0.006 nm^2 and 0.652 ± 0.006 nm^2, respectively, which decrease to 0.581 ± 0.008 nm^2 and 0.594 ± 0.008 nm^2 at the highest capsaicin concentration. Notably, the APL obtained for pure DPPC at 310 K is higher than expected for a gel-phase bilayer (≈0.45 nm^2),[111,112] suggesting a partially disordered state in the present simulations. Bilayer thicknesses for pure DPPC and POPC membranes are 3.742 ± 0.035 and 3.739 ± 0.032 nm, respectively, decreasing to 3.487 ± 0.038 and 3.541 ± 0.044 nm at a capsaicin-to-lipid ratio of 0.50. The effect of capsaicin in reducing the lipid bilayer thickness has also been reported in previous all-atom MD studies of DC18:1PC and DC22:1PC bilayers.[57] Consequently, the VPL decreases approximately linearly by up to 13.41% for DPPC and 13.70% for POPC at this ratio. In contrast, cholesterol at low concentrations reduces the area per lipid while increasing bilayer thickness,[41,42,53,105] and α-tocopherol has similarly been reported to induce an increase in the bilayer thickness.[113] These modest structural changes indicate that capsaicin has a small perturbation on bilayer volume or integrity, potentially acting as a membrane-active agent. It is compatible for loading into liposomal drug carriers without compromising the overall bilayer stability or barrier function.

Deuterium order parameter analysis (S_{CD}) shown on Figure 12. The S_{CD} profiles of DPPC and POPC bilayers show that capsaicin induces only modest changes in lipid tail ordering, primarily in the upper acyl chain region (around C1−C4), adjacent to the lipid ester groups. Notably, the S_{CD} of DPPC bilayer at 310 K is approximately 0.2, which is substantially lower than the characteristic value of 0.4 for the gel phase, indicating that DPPC is in the disordered phase rather than in the gel phase. This behavior had been shown in the comparative force field studies of DPPC bilayers.[114,115] The united atom model of DPPC bilayers, described with the GROMOS 54a7 force field, shift phase behavior and underestimate the acyl-chain ordering.[114,115] Consequently, the apparent impact of capsaicin on lipid ordering is limited, with the average S_{CD} decreasing by only 7.0% and 5.5% in the *sn*-1 and *sn*-2 chains, respectively, even at the highest capsaicin-to-lipid ratio (0.50). For the POPC bilayer, 310 K is above the melting temperature, and a liquid-disordered phase is well observed with an average S_{CD} of 0.141. The addition of capsaicin at the 0.5 capsaicin-to-lipid ratio has a small decrease of S_{CD} (1.9% and 0.5% for the *sn*-1 and *sn*-2 chains, respectively). The limited effect of capsaicin on the bilayer may result from a high fluid lipid in the disorder phase. To have a better understanding of the effect of capsaicin on the ordered bilayer, we perform additional DPPC simulations at extremely low temperatures of 273 K, in which pure DPPC lipids exhibit an ordered structure (gel-phase) with an average S_{CD} of 0.278. The visualization and S_{CD} analysis are shown in Figures S3 and S4. Interestingly, the S_{CD} rapidly decreases about 30% when 20% capsaicin is added in the bilayer. The significant disturbance of capsaicin in the chain order is in agreement with experimental studies of capsaicin-induced membrane fluidization.[38,39,94,116]

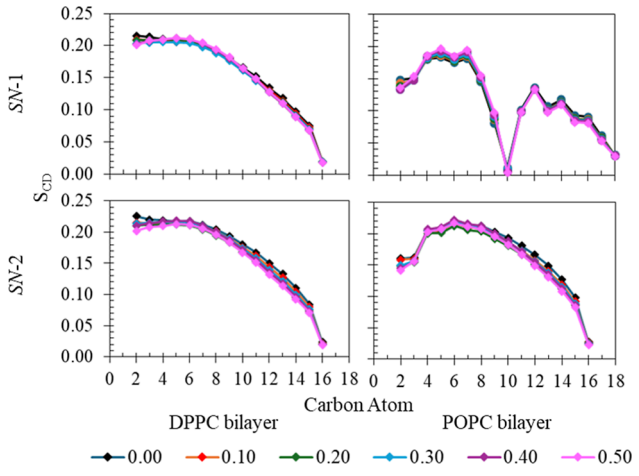

Figure 12. Deuterium order parameters (S_{CD}) of the lipid hydrocarbon tail *sn*-1 and *sn*-2 of the DPPC and POPC bilayers at varying capsaicin-to-lipid ratios. The line colors correspond to the different capsaicin-to-lipid ratios.

3.5. Permeability of Water across in the Lipid Bilayer

Water permeability across the lipid bilayer is a fundamental biophysical property that can be influenced by external factors, such as embedded molecules. Understanding the water permeability contributes to a more complete picture of how embedded molecules alter the biophysical characteristics and behavior of the membrane. To investigate the impact of capsaicin on water permeability (P_f), the water permeability coefficient of the lipid bilayer is calculated using Fick's Law and Flux-Based Counting method.[117−119] In this approach, P_f is derived directly from the number of water permeation events observed during the simulation. The equation is

$$P_f = \frac{\langle N_{permeate} \rangle}{2AtC_{bulk}} \quad (2)$$

where $N_{permeate}$ is the number of permeated water molecules during simulation time t, A is the cross-sectional area of lipid bilayer, and C_{bulk} is bulk water concentration, which is derived from the mass−density profiles (32 molecules per nm^3). The factor of 2 accounts for permeation events occurring in both directions across the bilayer. In the pure lipid systems, the number of water permeation events is 90 ± 7 in DPPC and 91 ± 7 in POPC, yielding the P_f of 1.6 ± 0.6 × 10^{-3} and 1.60 ± 0.5 × 10^{-3} cm/s, respectively. The values are in the same order of magnitude as in previous MD studies for pure DPPC (0.8−3.1 × 10^{-3} cm/s)[119,120] and POPC bilayers (1.5−2.1 × 10^{-3} cm/s).[118,121] To verify the robustness of our results, we performed two additional simulations of pure bilayers that consistently produced permeability coefficients in the same range. Consistent with typical atomistic MD results, the calculated permeability coefficients are lower than experimental measurements, owing to the limited number of permeation events captured within the accessible simulation time scales.[119]

https://doi.org/10.1021/acsomega.5c07901
ACS Omega 2026, 11, 23728−23742

Additionally, water permeability in simulations is sensitive to parameters including temperature, system size, and force field.[119−121] Upon embedding capsaicin, the number of water permeation events in the lipid bilayer increased slightly, ranging from 101 to 160 events, with no clear dependence on the capsaicin-to-lipid ratio. This yielded a P_f of 1.5−3.5 × 10^{-3} cm/s across all systems, as shown in Figure 13. Overall, the

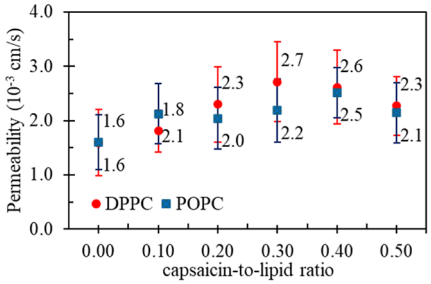

Figure 13. Water permeability coefficients of the DPPC and POPC lipid bilayers at varying capsaicin-to-lipid ratios. Error bars indicate fluctuations in water permeation events during the simulation.

weak and nonmonotonic changes in water permeability indicate that capsaicin incorporation does not substantially alter the membrane barrier function under the present simulation conditions.

4. CONCLUSIONS

In this study, we employed extensive atomistic molecular dynamics simulations to elucidate the translocation and membrane interactions of capsaicin in the POPC and DPPC bilayers. Our findings reveal a stepwise insertion mechanism, wherein the phenolic group of capsaicin initially anchors to the phosphate headgroups of the lipids through hydrogen bonding, followed by the hydrophobic tail flipping into the bilayer core. This adsorption and orientation process occurs more rapidly in POPC membranes than in DPPC, which can be attributed to the higher area per lipid. Whereas individual capsaicin molecules readily permeate the bilayer, small clusters stabilized by amide−amide interactions exhibit reduced membrane penetration, indicating that slow and low-concentration loading conditions are more favorable for efficient incorporation into the lipid bilayer. After translocation, capsaicin molecules predominantly localize near the lipid headgroup region. Their stability in this region is mediated by persistent phenol-phosphate and occasional amide-ester hydrogen bonds. At higher concentrations, capsaicin molecules exhibit enhanced self-association into small clusters such as dimers and trimers; yet, large aggregates are not observed, and most molecules remain in a monomeric state within the membrane even at the highest concentrations studied.

Interestingly, area per lipid and bilayer thickness exhibit small concentration-dependent changes, and lipid chain order is weakly affected when membranes are already in a partially disordered state. In contrast, additional simulations performed on highly ordered DPPC bilayers reveal a clear capsaicin-induced disordering transition at higher concentrations, consistent with experimental observations of membrane fluidization and underscore the critical role of membrane phase state in interpreting simulation outcomes. In agreement with these observations, water permeability does not show a strong or systematic dependence on the capsaicin concentration, indicating that capsaicin incorporation does not substantially compromise the membrane barrier to water under the present simulation conditions.

Together, this work provides molecular-level insights into capsaicin−lipid interactions that bridge experimental observations with a mechanistic understanding. Our simulation results support the feasibility of liposomal encapsulation as a strategy to improve capsaicin bioavailability and provide a molecular-level explanation for optimizing membrane-based delivery systems for small amphiphilic bioactive compounds.

■ ASSOCIATED CONTENT

Supporting Information

The Supporting Information is available free of charge at https://pubs.acs.org/doi/10.1021/acsomega.5c07901.

Side-view snapshots of initial and final configurations at 200 ns from atomistic MD simulations of a single capsaicin in the DPPC and POPC bilayers, complete 200 ns time evolution of capsaicin insertion dynamics in DPPC and POPC bilayers from single-capsaicin simulations, side-view snapshots of final configurations from the additional simulations of DPPC at 273 K, and average deuterium order parameters (S_{CD}) of the DPPC bilayer from additional simulations at 273 K, compared with the main simulation at 310 K (PDF)

■ AUTHOR INFORMATION

Corresponding Author

Jirasak Wong-ekkabut − *Department of Physics, Faculty of Science, Kasetsart University, Bangkok 10900, Thailand; Computational Biomodelling Laboratory for Agricultural Science and Technology (CBLAST), Faculty of Science, Kasetsart University, Bangkok 10900, Thailand;* orcid.org/0000-0002-3651-9870; Email: jirasak.w@ku.th

Authors

Nathanon Kerdkaen − *Department of Physics, Faculty of Science, Kasetsart University, Bangkok 10900, Thailand; Computational Biomodelling Laboratory for Agricultural Science and Technology (CBLAST), Faculty of Science, Kasetsart University, Bangkok 10900, Thailand*

Nililla Nisoh − *Department of Physics, Faculty of Science, Kasetsart University, Bangkok 10900, Thailand; Computational Biomodelling Laboratory for Agricultural Science and Technology (CBLAST), Faculty of Science, Kasetsart University, Bangkok 10900, Thailand*

Jiramate Kitjanon − *Department of Physics, Faculty of Science, Kasetsart University, Bangkok 10900, Thailand; Computational Biomodelling Laboratory for Agricultural Science and Technology (CBLAST), Faculty of Science, Kasetsart University, Bangkok 10900, Thailand*

Cristiano Dias − *Department of Physics, New Jersey Institute of Technology, Newark, New Jersey 07102-1982, United States;* orcid.org/0000-0002-8765-3922

Mikko Karttunen − *European Laboratory for Learning and Intelligent Systems (ELLIS) Institute Finland, 02150 Espoo, Finland; Department of Technical Physics, University of Eastern Finland, FI-70211 Kuopio, Finland;* orcid.org/0000-0002-8626-3033

Complete contact information is available at: https://pubs.acs.org/10.1021/acsomega.5c07901

https://doi.org/10.1021/acsomega.5c07901
ACS Omega 2026, 11, 23728−23742

Notes

The authors declare no competing financial interest.

■ ACKNOWLEDGMENTS

This work was financially supported by National Research Council of Thailand (NRCT) and A-STAR INNOVATION COMPANY LIMITED [Grant No. N41A650168] (JW and NK). NN and JW are supported by the National Science Research and Innovation Fund (NSRF) via the Program Management Unit for Human Resources & Institutional Development Research and Innovation (PMUB) [Grant No. B13F660122, B11F670109, and B42G670041]. The network collaboration between MK and JW research groups is supported the Nordic Alumni Engagement Initiative at Kasetsart University. MK also thanks Foundation PS for financial support.

■ REFERENCES

(1) McCormack, P. L. Capsaicin Dermal Patch: In Non-Diabetic Peripheral Neuropathic Pain. *Drugs* **2010**, *70* (14), 1831−1842.
(2) Chapa-Oliver, A. M.; Mejía-Teniente, L. Capsaicin: From Plants to a Cancer-Suppressing Agent. *Molecules* **2016**, *21* (8), 931.
(3) Blair, H. A. Capsaicin 8% Dermal Patch: A Review in Peripheral Neuropathic Pain. *Drugs* **2018**, *78* (14), 1489−1500.
(4) Friedman, J. R.; Nolan, N. A.; Brown, K. C.; Miles, S. L.; Akers, A. T.; Colclough, K. W.; Seidler, J. M.; Rimoldi, J. M.; Valentovic, M. A.; Dasgupta, P. Anticancer Activity of Natural and Synthetic Capsaicin Analogs. *J. Pharmacol. Exp. Ther.* **2018**, *364* (3), 462−473.
(5) Lu, M.; Chen, C.; Lan, Y.; Xiao, J.; Li, R.; Huang, J.; Huang, Q.; Cao, Y.; Ho, C. T. Capsaicin-the Major Bioactive Ingredient of Chili Peppers: Bio-Efficacy and Delivery Systems. *Food Funct.* **2020**, *11* (4), 2848−2860.
(6) Arora, V.; Campbell, J. N.; Chung, M.-K. Fight Fire with Fire: Neurobiology of Capsaicin-Induced Analgesia for Chronic Pain. *Pharmacol. Ther.* **2021**, *220*, 107743.
(7) Adetunji, T. L.; Olawale, F.; Olisah, C.; Adetunji, A. E.; Aremu, A. O. Capsaicin: A Two-Decade Systematic Review of Global Research Output and Recent Advances against Human Cancer. *Front. Oncol.* **2022**, *12*, 908487.
(8) Maharjan, A.; Vasamsetti, B. M. K.; Park, J.-H. A Comprehensive Review of Capsaicin: Biosynthesis, Industrial Productions, Processing to Applications, and Clinical Uses. *Heliyon* **2024**, *10* (21), No. e39721.
(9) Hayman, M.; Kam, P. C. A. Capsaicin: A Review of Its Pharmacology and Clinical Applications. *Anaesth. Intensive Care* **2008**, *19* (5), 338−343.
(10) Rollyson, W. D.; Stover, C. A.; Brown, K. C.; Perry, H. E.; Stevenson, C. D.; McNees, C. A.; Ball, J. G.; Valentovic, M. A.; Dasgupta, P. Bioavailability of Capsaicin and Its Implications for Drug Delivery. *J. Controlled Release* **2014**, *196*, 96−105.
(11) Chung, M.-K.; Campbell, J. N. Use of Capsaicin to Treat Pain: Mechanistic and Therapeutic Considerations. *Pharmaceuticals* **2016**, *9* (4), 66.
(12) Fattori, V.; Hohmann, M. S.; Rossaneis, A. C.; Pinho-Ribeiro, F. A.; Verri, W. A. Capsaicin: Current Understanding of Its Mechanisms and Therapy of Pain and Other Pre-Clinical and Clinical Uses. *Molecules* **2016**, *21* (7), 844.
(13) Anand, P.; Bley, K. Topical Capsaicin for Pain Management: Therapeutic Potential and Mechanisms of Action of the New High-Concentration Capsaicin 8 Patch. *Br. J. Anaesth.* **2011**, *107*, 490−502.
(14) Derry, S.; Rice, A. S.; Cole, P.; Tan, T.; Moore, R. A. Topical Capsaicin (High Concentration) for Chronic Neuropathic Pain in Adults. *Cochrane. Database Syst. Rev.* **2017**, *2021* (7), Cd007393.
(15) Thomas, S. E.; Laycock, H. The Use of High Dose Topical Capsaicin in the Management of Peripheral Neuropathy: Narrative Review and Local Experience. *British Journal of Pain* **2020**, *14* (2), 133−140.
(16) Yang, X. D.; Fang, P. F.; Xiang, D. X.; Yang, Y. Y. Treatment of Painful Diabetic Neuropathy with Topical Capsaicin: A Multicenter, Double-Blind, Vehicle-Controlled Study. *Arch. Intern. Med.* **1991**, *151* (11), 2225−2229.
(17) Kulkantrakorn, K.; Lorsuwansiri, C.; Meesawatsom, P. 0.025% Capsaicin Gel for the Treatment of Painful Diabetic Neuropathy: A Randomized, Double-Blind, Crossover, Placebo-Controlled Trial. *Pain Practice* **2013**, *13* (6), 497−503.
(18) Yang, X. D.; Fang, P. F.; Xiang, D. X.; Yang, Y. Y. Topical Treatments for Diabetic Neuropathic Pain. *Exp. Ther. Med.* **2019**, *17* (3), 1963−1976.
(19) Agoons, B. B.; Dehayem Yefou, M.; Katte, J. C.; Etoa Etoga, M. C.; Agoons, D. D.; Yepnjio, F.; Boli, A.; Wasnyo, Y.; Sobngwi, E.; Mbanya, J. C. Effect of Topical Capsaicin on Painful Sensory Peripheral Neuropathy in Patients with Type 2 Diabetes: A Double-Blind Placebo-Controlled Randomised Clinical Trial. *Cureus* **2020**, *12* (10), No. e11147.
(20) Goodwin, B.; Chiplunkar, M.; Salerno, R.; Coombs, K.; Sannoh, U.; Shah, V.; Averell, N.; Al-Shebab, U.; Janora, D. Topical Capsaicin for the Management of Painful Diabetic Neuropathy: A Narrative Systematic Review. *Pain Manage.* **2023**, *13* (5), 309−316.
(21) Simpson, D. M.; Robinson-Papp, J.; Van, J.; Stoker, M.; Jacobs, H.; Snijder, R. J.; Schregardus, D. S.; Long, S. K.; Lambourg, B.; Katz, N. Capsaicin 8% Patch in Painful Diabetic Peripheral Neuropathy: A Randomized, Double-Blind, Placebo-Controlled Study. *J. Pain* **2017**, *18* (1), 42−53.
(22) Anand, P.; Privitera, R.; Donatien, P.; Fadavi, H.; Tesfaye, S.; Bravis, V.; Misra, V. P. Reversing Painful and Non-Painful Diabetic Neuropathy with the Capsaicin 8% Patch: Clinical Evidence for Pain Relief and Restoration of Function Via Nerve Fiber Regeneration. *Front. Neuro.* **2022**, *13*, 998904.
(23) Goodwin, B.; Chiplunkar, M.; Salerno, R.; Coombs, K.; Sannoh, U.; Shah, V.; Averell, N.; Al-Shebab, U.; Janora, D. Topical Capsaicin for the Management of Painful Diabetic Neuropathy: A Narrative Systematic Review. *Pain Manage.* **2023**, *13* (5), 309−316.
(24) Wong, G. Y.; Gavva, N. R. Therapeutic Potential of Vanilloid Receptor Trpv1 Agonists and Antagonists as Analgesics: Recent Advances and Setbacks. *Brain Res. Rev.* **2009**, *60* (1), 267−277.
(25) Giaccari, L. G.; Aurilio, C.; Coppolino, F.; Pace, M. C.; Passsavanti, M. B.; Pota, V.; Sansone, P. Capsaicin 8% Patch and Chronic Postsurgical Neuropathic Pain. *J. Pers. Med.* **2021**, *11* (10), 960.
(26) Goodwin, B.; Mitchell, J.; Major, E.; Podwojniak, A.; Brancaccio, H.; Rusinak, K.; King, M.; Tahir, H. The Efficacy of Topical 8% Capsaicin Patches for the Treatment of Postsurgical Neuropathic Pain: A Systematic Review. *Pain Manage.* **2024**, *14* (10−11), 591−598.
(27) Feng, Y.; Zhu, Y.; Wan, J.; Yang, X.; Firempong, C. K.; Yu, J.; Xu, X. Enhanced Oral Bioavailability, Reduced Irritation and Increased Hypolipidemic Activity of Self-Assembled Capsaicin Prodrug Nanoparticles. *J. Funct. Foods* **2018**, *44*, 137−145.
(28) Puri, A.; Loomis, K.; Smith, B.; Lee, J. H.; Yavlovich, A.; Heldman, E.; Blumenthal, R. Lipid-Based Nanoparticles as Pharmaceutical Drug Carriers: From Concepts to Clinic. *Crit. Rev. Ther. Drug Carrier Syst.* **2009**, *26* (6), 523−580.
(29) Tester, C. C.; Brock, R. E.; Wu, C.-H.; Krejci, M. R.; Weigand, S.; Joester, D. In Vitro Synthesis and Stabilization of Amorphous Calcium Carbonate (Acc) Nanoparticles within Liposomes. *CrystEngComm* **2011**, *13* (12), 3975−3978.
(30) Slingerland, M.; Guchelaar, H. J.; Gelderblom, H. Liposomal Drug Formulations in Cancer Therapy: 15 Years Along the Road. *Drug Discovery Today* **2012**, *17* (3−4), 160−166.
(31) Bozzuto, G.; Molinari, A. Liposomes as Nanomedical Devices. *Int. J. Nanomed.* **2015**, *10*, 975−999.
(32) Bunker, A.; Magarkar, A.; Viitala, T. Rational Design of Liposomal Drug Delivery Systems, a Review: Combined Experimental and Computational Studies of Lipid Membranes, Liposomes and Their Pegylation. *Biochim. Biophys. Acta, Biomembr.* **2016**, *1858* (10), 2334−2352.

https://doi.org/10.1021/acsomega.5c07901
ACS Omega 2026, 11, 23728−23742

(33) Luo, M.; Oomah, B. D.; Akoetey, W.; Zhang, Y.; Daneshfozoun, H.; Hosseinian, F. Liposomes as Sustainable Delivery Systems in Food, Cosmetic, and Pharmaceutical Applications. *Journal of the American Oil Chemists' Society* **2025**, *102* (3), 547−568.
(34) Zhu, Y.; Wang, M.; Zhang, J.; Peng, W.; Firempong, C. K.; Deng, W.; Wang, Q.; Wang, S.; Shi, F.; Yu, J.; et al. Improved Oral Bioavailability of Capsaicin Via Liposomal Nanoformulation: Preparation, in Vitro Drug Release and Pharmacokinetics in Rats. *Arch. Pharmacal Res.* **2015**, *38* (4), 512−521.
(35) Giri, T. K.; Mukherjee, P.; Barman, T. K.; Maity, S. Nano-Encapsulation of Capsaicin on Lipid Vesicle and Evaluation of Their Hepatocellular Protective Effect. *Int. J. Biol. Macromol.* **2016**, *88*, 236−243.
(36) Al-Samydai, A.; Alshaer, W.; Al-Dujaili, E. A. S.; Azzam, H.; Aburjai, T. Preparation, Characterization, and Anticancer Effects of Capsaicin-Loaded Nanoliposomes. *Nutrients* **2021**, *13* (11), 3995.
(37) Swain, J.; Kumar Mishra, A. Location, Partitioning Behavior, and Interaction of Capsaicin with Lipid Bilayer Membrane: Study Using Its Intrinsic Fluorescence. *J. Phys. Chem. B* **2015**, *119* (36), 12086−12093.
(38) Torrecillas, A.; Schneider, M.; Fernández-Martínez, A. M.; Ausili, A.; de Godos, A. M.; Corbalán-García, S.; Gómez-Fernández, J. C. Capsaicin Fluidifies the Membrane and Localizes Itself near the Lipid−Water Interface. *ACS Chem. Neurosci.* **2015**, *6* (10), 1741−1750.
(39) Geraldo, V. P. N.; Ziglio, A. C.; Gonçalves, D.; Oliveira, O. N. Interaction of Capsaicinoids with Cell Membrane Models Does Not Correlate with Pungency of Peppers. *Chem. Phys. Lett.* **2017**, *673*, 78−83.
(40) Juárez-Contreras, R.; Mota-Carrillo, E.; Piedra-Ramírez, A.; Farías-Sánchez, D.; González-Ramírez, R.; Morales-Lázaro, S. L. Capsaicin: Beyond Trpv1. *Front. Nutr.* **2025**, *12*, 1594742.
(41) Hofsäss, C.; Lindahl, E.; Edholm, O. Molecular Dynamics Simulations of Phospholipid Bilayers with Cholesterol. *Biophys. J.* **2003**, *84* (4), 2192−2206.
(42) de Meyer, F.; Smit, B. Effect of Cholesterol on the Structure of a Phospholipid Bilayer. *Proc. Natl. Acad. Sci. U. S. A.* **2009**, *106* (10), 3654−3658.
(43) Karami, L.; Jalili, S. Effects of Cholesterol Concentration on the Interaction of Cytarabine with Lipid Membranes: A Molecular Dynamics Simulation Study. *J. Biomol. Struct. Dyn.* **2015**, *33* (6), 1254−1268.
(44) Marquardt, D.; Kučerka, N.; Wassall, S. R.; Harroun, T. A.; Katsaras, J. Cholesterol's Location in Lipid Bilayers. *Chem. Phys. Lipids* **2016**, *199*, 17−25.
(45) Khuntawee, W.; Wolschann, P.; Rungrotmongkol, T.; Wong-ekkabut, J.; Hannongbua, S. Molecular Dynamics Simulations of the Interaction of Beta Cyclodextrin with a Lipid Bilayer. *J. Chem. Inf. Model.* **2015**, *55* (9), 1894−1902.
(46) Boonnoy, P.; Karttunen, M.; Wong-ekkabut, J. Alpha-Tocopherol Inhibits Pore Formation in Oxidized Bilayers. *Phys. Chem. Chem. Phys.* **2017**, *19* (8), 5699−5704.
(47) Khuntawee, W.; Karttunen, M.; Wong-ekkabut, J. A Molecular Dynamics Study of Conformations of Beta-Cyclodextrin and Its Eight Derivatives in Four Different Solvents. *Phys. Chem. Chem. Phys.* **2017**, *19* (35), 24219−24229.
(48) Boonnoy, P.; Karttunen, M.; Wong-ekkabut, J. Does A-Tocopherol Flip-Flop Help to Protect Membranes against Oxidation? *J. Phys. Chem. B* **2018**, *122* (45), 10362−10370.
(49) De Paula, E.; Pickholz, M.; Albano, J. In *Molecular Dynamics Simulations to Study Drug Delivery Systems. Molecular Dynamics*; Vakhrushev, A. V., Ed.; IntechOpen, 2018.
(50) Nisoh, N.; Jarerattanachat, V.; Karttunen, M.; Wong-ekkabut, J. Formation of Aggregates, Icosahedral Structures and Percolation Clusters of Fullerenes in Lipids Bilayers: The Key Role of Lipid Saturation. *Biochim. Biophys. Acta, Biomembr.* **2020**, *1862* (9), 183328.
(51) Hashemzadeh, H.; Javadi, H.; Darvishi, M. H. Study of Structural Stability and Formation Mechanisms in Dspc and Dpsm Liposomes: A Coarse-Grained Molecular Dynamics Simulation. *Sci. Rep.* **2020**, *10* (1), 1837.
(52) Khuntawee, W.; Amornloetwattana, R.; Vongsangnak, W.; Namdee, K.; Yata, T.; Karttunen, M.; Wong-ekkabut, J. In Silico and in Vitro Design of Cordycepin Encapsulation in Liposomes for Colon Cancer Treatment. *RSC Adv.* **2021**, *11* (15), 8475−8484.
(53) Boonnoy, P.; Janlad, M.; Bagheri, B.; Dias, C.; Karttunen, M.; Wong-ekkabut, J. Cholesterol Inhibits Oxygen Permeation through Biological Membranes: Mechanism against Double-Bond Peroxidation. *RSC Adv.* **2024**, *14* (40), 29113−29121.
(54) Nisoh, N.; Jarerattanachat, V.; Dias, C.; Wong-Ekkabut, J. Insight into the Interactions of Fullerenes with Biological Membranes through Molecular Dynamics Simulations. *Adv. Phys.:X* **2024**, *9* (1), 2350160.
(55) Hanson, S. M.; Newstead, S.; Swartz, K. J.; Sansom, M. S. P. Capsaicin Interaction with Trpv1 Channels in a Lipid Bilayer: Molecular Dynamics Simulation. *Biophys. J.* **2015**, *108* (6), 1425−1434.
(56) Yang, F.; Zheng, J. Understand Spiciness: Mechanism of Trpv1 Channel Activation by Capsaicin. *Protein Cell* **2017**, *8* (3), 169−177.
(57) Sun, D.; Peyear, T. A.; Bennett, W. F. D.; Holcomb, M.; He, S.; Zhu, F.; Lightstone, F. C.; Andersen, O. S.; Ingólfsson, H. I. Assessing the Perturbing Effects of Drugs on Lipid Bilayers Using Gramicidin Channel-Based in Silico and in Vitro Assays. *J. Med. Chem.* **2020**, *63* (20), 11809−11818.
(58) Domene, C.; Darré, L.; Oakes, V.; Gonzalez-Resines, S. A Potential Route of Capsaicin to Its Binding Site in the Trpv1 Ion Channel. *J. Chem. Inf. Model.* **2022**, *62* (10), 2481−2489.
(59) Lambert, J. W.; Sum, A. K. Molecular Dynamics Study of the Properties of Capsaicin in an 1-Octanol/Water System. *J. Phys. Chem. B* **2006**, *110* (5), 2351−2357.
(60) Ingólfsson, H. I.; Thakur, P.; Herold, K. F.; Hobart, E. A.; Ramsey, N. B.; Periole, X.; de Jong, D. H.; Zwama, M.; Yilmaz, D.; Hall, K.; et al. Phytochemicals Perturb Membranes and Promiscuously Alter Protein Function. *ACS Chem. Biol.* **2014**, *9* (8), 1788−1798.
(61) Poger, D.; Mark, A. E. On the Validation of Molecular Dynamics Simulations of Saturated and Cis-Monounsaturated Phosphatidylcholine Lipid Bilayers: A Comparison with Experiment. *J. Chem. Theory Comput.* **2010**, *6* (1), 325−336.
(62) Poger, D.; Van Gunsteren, W. F.; Mark, A. E. A New Force Field for Simulating Phosphatidylcholine Bilayers. *J. Comput. Chem.* **2010**, *31* (6), 1117−1125.
(63) Schmid, N.; Eichenberger, A. P.; Choutko, A.; Riniker, S.; Winger, M.; Mark, A. E.; van Gunsteren, W. F. Definition and Testing of the Gromos Force-Field Versions 54a7 and 54b7. *Eur. Biophys. J.* **2011**, *40* (7), 843−856.
(64) Malde, A. K.; Zuo, L.; Breeze, M.; Stroet, M.; Poger, D.; Nair, P. C.; Oostenbrink, C.; Mark, A. E. An Automated Force Field Topology Builder (Atb) and Repository: Version 1.0. *J. Chem. Theory Comput.* **2011**, *7* (12), 4026−4037.
(65) Stroet, M.; Caron, B.; Visscher, K. M.; Geerke, D. P.; Malde, A. K.; Mark, A. E. Automated Topology Builder Version 3.0: Prediction of Solvation Free Enthalpies in Water and Hexane. *J. Chem. Theory Comput.* **2018**, *14* (11), 5834−5845.
(66) Tieleman, D. P.; Berendsen, H. J. C. Molecular Dynamics Simulations of a Fully Hydrated Dipalmitoylphosphatidylcholine Bilayer with Different Macroscopic Boundary Conditions and Parameters. *J. Chem. Phys.* **1996**, *105* (11), 4871−4880.
(67) Knight, C. J.; Hub, J. S. Memgen: A General Web Server for the Setup of Lipid Membrane Simulation Systems. *Bioinformatics* **2015**, *31* (17), 2897−2899.
(68) Berendsen, H.; Postma, J. P. M.; van Gunsteren, W.; Hermans, J. Interaction Models for Water in Relation to Protein Hydration. In: Pullman, B.. (eds) *Intermolecular Forces. The Jerusalem Symposia on Quantum Chemistry and Biochemistry*, vol *14*. Springer, Dordrecht. .
(69) Bennett, W. F. D.; Tieleman, D. P. Water Defect and Pore Formation in Atomistic and Coarse-Grained Lipid Membranes:

https://doi.org/10.1021/acsomega.5c07901
ACS Omega 2026, 11, 23728−23742

Pushing the Limits of Coarse Graining. *J. Chem. Theory Comput.* **2011**, *7* (9), 2981−2988.
(70) Pourmousa, M.; Wong-ekkabut, J.; Patra, M.; Karttunen, M. Molecular Dynamic Studies of Transportan Interacting with a Dppc Lipid Bilayer. *J. Phys. Chem. B* **2013**, *117* (1), 230−241.
(71) Abraham, M. J.; Murtola, T.; Schulz, R.; Páll, S.; Smith, J. C.; Hess, B.; Lindahl, E. Gromacs: High Performance Molecular Simulations through Multi-Level Parallelism from Laptops to Supercomputers. *SoftwareX* **2015**, *1−2*, 19−25.
(72) Páll, S.; Abraham, M. J.; Kutzner, C.; Hess, B.; Lindahl, E. Tackling Exascale Software Challenges in Molecular Dynamics Simulations with Gromacs. In *Solving Software Challenges for Exascale*; Markidis, S., Laure, E., Eds.; Springer International Publishing: Cham, 2015; pp 3−27.
(73) Parrinello, M.; Rahman, A. Polymorphic Transitions in Single Crystals: A New Molecular Dynamics Method. *J. Appl. Phys.* **1981**, *52* (12), 7182−7190.
(74) Bussi, G.; Donadio, D.; Parrinello, M. Canonical Sampling through Velocity Rescaling. *J. Chem. Phys.* **2007**, *126* (1), 014101.
(75) Darden, T.; York, D.; Pedersen, L. Particle Mesh Ewald: An N·Log(N) Method for Ewald Sums in Large Systems. *J. Chem. Phys.* **1993**, *98* (12), 10089−10092.
(76) Essmann, U.; Perera, L.; Berkowitz, M. L.; Darden, T.; Lee, H.; Pedersen, L. G. A Smooth Particle Mesh Ewald Method. *J. Chem. Phys.* **1995**, *103* (19), 8577−8593.
(77) Karttunen, M.; Rottler, J.; Vattulainen, I.; Sagui, C. Electrostatics in Biomolecular Simulations: Where Are We Now and Where Are We Heading? *Curr. Top. Membr.* **2008**, *60*, 49.
(78) Hess, B. P.-L. A Parallel Linear Constraint Solver for Molecular Simulation. *J. Chem. Theory Comput.* **2008**, *4* (1), 116−122.
(79) Humphrey, W.; Dalke, A.; Schulten, K. Vmd: Visual Molecular Dynamics. *J. Mol. Graphics* **1996**, *14* (1), 33−38.
(80) Polvat, T.; Khuntawee, W.; Prasertporn, T.; Promthep, K.; Kerdkaen, N.; Panmanee, J.; Nalakarn, P.; Wong-ekkabut, J.; Chetsawang, B. The Potential Mechanism of Methamphetamine-Induced Mitochondrial Dysfunction and Cell Degeneration Via Direct Permeation across Mitochondrial Membranes: The Study on Molecular Dynamics Simulations and in Vitro Model. *Food Chem. Toxicol.* **2025**, *206*, 115743.
(81) Wong-ekkabut, J.; Karttunen, M. The Good, the Bad and the User in Soft Matter Simulations. *Biochim. Biophys. Acta, Biomembr.* **2016**, *1858* (10), 2529−2538.
(82) Wong-ekkabut, J.; Karttunen, M. Molecular Dynamics Simulation of Water Permeation through the Alpha-Hemolysin Channel. *J. Biol. Phys.* **2016**, *42* (1), 133−146.
(83) Lukat, G.; Krüger, J.; Sommer, B. Apl@Voro: A Voronoi-Based Membrane Analysis Tool for Gromacs Trajectories. *J. Chem. Inf. Model.* **2013**, *53* (11), 2908−2925.
(84) Kern, M.; Jaeger-Honz, S.; Schreiber, F.; Sommer, B. Apl@Voro—Interactive Visualization and Analysis of Cell Membrane Simulations. *Bioinformatics* **2023**, *39* (2), btad083.
(85) Bartoš, L.; Pajtinka, P.; Vácha, R. G. Comprehensive Tool for Calculating Lipid Order Parameters from Molecular Simulations. *SoftwareX* **2025**, *31*, 102254.
(86) Rossum, G. V.; Drake, F. L. *Python 3 Reference Manual*; CreateSpace 2009.
(87) Harris, C. R.; Millman, K. J.; van der Walt, S. J.; Gommers, R.; Virtanen, P.; Cournapeau, D.; Wieser, E.; Taylor, J.; Berg, S.; Smith, N. J.; et al. Array Programming with Numpy. *Nature* **2020**, *585* (7825), 357−362.
(88) Michaud-Agrawal, N.; Denning, E. J.; Woolf, T. B.; Beckstein, O. Mdanalysis: A Toolkit for the Analysis of Molecular Dynamics Simulations. *J. Comput. Chem.* **2011**, *32* (10), 2319−2327.
(89) Gowers, R. J.; Linke, M.; Barnoud, J.; Reddy, T. J. E.; Melo, M. N.; Seyler, S. L.; Domanski, J.; Dotson, D. L.; Buchoux, S.; Kenney, I. M.; Beckstein, O. Mdanalysis: A Python Package for the Rapid Analysis of Molecular Dyna Mics Simulations. In *Python in Science Conference*, Benthall, 2016; pp 98−105..
(90) Marrink, S. J.; Berendsen, H. J. C. Permeation Process of Small Molecules across Lipid Membranes Studied by Molecular Dynamics Simulations. *J. Phys. Chem.* **1996**, *100* (41), 16729−16738.
(91) Wong-ekkabut, J.; Xu, Z.; Triampo, W.; Tang, I. M.; Peter Tieleman, D.; Monticelli, L. Effect of Lipid Peroxidation on the Properties of Lipid Bilayers: A Molecular Dynamics Study. *Biophys. J.* **2007**, *93* (12), 4225−4236.
(92) Basith, S.; Cui, M.; Hong, S.; Choi, S. Harnessing the Therapeutic Potential of Capsaicin and Its Analogues in Pain and Other Diseases. *Molecules* **2016**, *21* (8), 966.
(93) Ilie, M. A.; Caruntu, C.; Tampa, M.; Georgescu, S. R.; Matei, C.; Negrei, C.; Ion, R. M.; Constantin, C.; Neagu, M.; Boda, D. Capsaicin: Physicochemical Properties, Cutaneous Reactions and Potential Applications in Painful and Inflammatory Conditions. *Exp. Ther. Med.* **2019**, *18* (2), 916−925.
(94) Sharma, N.; Phan, H. T. T.; Yoda, T.; Shimokawa, N.; Vestergaard, M. C.; Takagi, M. Effects of Capsaicin on Biomimetic Membranes. *Biomimetics* **2019**, *4* (1), 17.
(95) Kim, S.; Chen, J.; Cheng, T.; Gindulyte, A.; He, J.; He, S.; Li, Q.; Shoemaker, B. A.; Thiessen, P. A.; Yu, B.; et al. Pubchem 2025 Update. *Nucleic Acids Res.* **2025**, *53* (D1), D1516−D1525.
(96) Pinisetty, D.; Moldovan, D.; Devireddy, R. The Effect of Methanol on Lipid Bilayers: An Atomistic Investigation. *Ann. Biomed. Eng.* **2006**, *34* (9), 1442−1451.
(97) Leekumjorn, S.; Sum, A. K. Molecular Characterization of Gel and Liquid-Crystalline Structures of Fully Hydrated Popc and Pope Bilayers. *J. Phys. Chem. B* **2007**, *111* (21), 6026−6033.
(98) Nalakarn, P.; Boonnoy, P.; Nisoh, N.; Karttunen, M.; Wong-ekkabut, J. Dependence of Fullerene Aggregation on Lipid Saturation Due to a Balance between Entropy and Enthalpy. *Sci. Rep.* **2019**, *9* (1), 1037.
(99) Bagheri, B.; Boonnoy, P.; Wong-ekkabut, J.; Karttunen, M. Effect of Oxidation on Popc Lipid Bilayers: Anionic Carboxyl Group Plays a Major Role. *Phys. Chem. Chem. Phys.* **2023**, *25* (27), 18310−18321.
(100) Luzar, A.; Chandler, D. Hydrogen-Bond Kinetics in Liquid Water. *Nature* **1996**, *379* (6560), 55−57.
(101) Dannenberg, J. J. An Introduction to Hydrogen Bonding by George A. Jeffrey (University of Pittsburgh). *J. Am. Chem. Soc.* **1998**, *120* (22), 5604.
(102) Kajander, T.; Kahn, P. C.; Passila, S. H.; Cohen, D. C.; Lehtiö, L.; Adolfsen, W.; Warwicker, J.; Schell, U.; Goldman, A. Buried Charged Surface in Proteins. *Structure* **2000**, *8* (11), 1203−1214.
(103) Kumar, S.; Rosenberg, J. M.; Bouzida, D.; Swendsen, R. H.; Kollman, P. A. The Weighted Histogram Analysis Method for Free-Energy Calculations on Biomolecules. I. The Method. *J. Comput. Chem.* **1992**, *13* (8), 1011−1021.
(104) Hub, J. S.; de Groot, B. L.; van der Spoel, D. G_Wham—a Free Weighted Histogram Analysis Implementation Including Robust Error and Autocorrelation Estimates. *J. Chem. Theory Comput.* **2010**, *6* (12), 3713−3720.
(105) Favela-Rosales, F.; Galván-Hernández, A.; Hernández-Cobos, J.; Kobayashi, N.; Carbajal-Tinoco, M. D.; Nakabayashi, S.; Ortega-Blake, I. A Molecular Dynamics Study Proposing the Existence of Statistical Structural Heterogeneity Due to Chain Orientation in the Popc-Cholesterol Bilayer. *Biophys. Chem.* **2020**, *257*, 106275.
(106) Jalili, S.; Saeedi, M. Study of Curcumin Behavior in Two Different Lipid Bilayer Models of Liposomal Curcumin Using Molecular Dynamics Simulation. *J. Biomol. Struct. Dyn.* **2016**, *34* (2), 327−340.
(107) Lyu, Y.; Xiang, N.; Mondal, J.; Zhu, X.; Narsimhan, G. Characterization of Interactions between Curcumin and Different Types of Lipid Bilayers by Molecular Dynamics Simulation. *J. Phys. Chem. B* **2018**, *122* (8), 2341−2354.
(108) Ileri Ercan, N. Understanding Interactions of Curcumin with Lipid Bilayers: A Coarse-Grained Molecular Dynamics Study. *J. Chem. Inf. Model.* **2019**, *59* (10), 4413−4426.
(109) Leng, X.; Kinnun, J. J.; Marquardt, D.; Ghefli, M.; Kučerka, N.; Katsaras, J.; Atkinson, J.; Harroun, T. A.; Feller, S. E.; Wassall, S.

https://doi.org/10.1021/acsomega.5c07901
ACS Omega 2026, 11, 23728−23742

R. A-Tocopherol Is Well Designed to Protect Polyunsaturated Phospholipids: Md Simulations. *Biophys. J.* **2015**, *109* (8), 1608−1618.
(110) Ausili, A.; Torrecillas, A.; de Godos, A. M.; Corbalán-García, S.; Gómez-Fernández, J. C. Phenolic Group of A-Tocopherol Anchors at the Lipid-Water Interface of Fully Saturated Membranes. *Langmuir* **2018**, *34* (10), 3336−3348.
(111) Sun, W. J.; Tristram-Nagle, S.; Suter, R. M.; Nagle, J. F. Structure of Gel Phase Saturated Lecithin Bilayers: Temperature and Chain Length Dependence. *Biophys. J.* **1996**, *71* (2), 885−891.
(112) Nagle, J. F.; Cognet, P.; Dupuy, F. G.; Tristram-Nagle, S. Structure of Gel Phase Dppc Determined by X-Ray Diffraction. *Chem. Phys. Lipids* **2019**, *218*, 168−177.
(113) DiPasquale, M.; Nguyen, M. H. L.; Pabst, G.; Marquardt, D. Partial Volumes of Phosphatidylcholines and Vitamin E: A-Tocopherol Prefers Disordered Membranes. *J. Phys. Chem. B* **2022**, *126* (35), 6691−6699.
(114) Pluhackova, K.; Kirsch, S. A.; Han, J.; Sun, L.; Jiang, Z.; Unruh, T.; Böckmann, R. A. A Critical Comparison of Biomembrane Force Fields: Structure and Dynamics of Model Dmpc, Popc, and Pope Bilayers. *J. Phys. Chem. B* **2016**, *120* (16), 3888−3903.
(115) Piggot, T. J.; Piñeiro, A.; Khalid, S. Correction to Molecular Dynamics Simulations of Phosphatidylcholine Membranes: A Comparative Force Field Study. *J. Chem. Theory Comput.* **2017**, *13* (4), 1862−1865.
(116) Mizogami, M.; Tsuchiya, H. Membrane Interactivity of Capsaicin Antagonized by Capsazepine. *Int. J. Mol. Sci.* **2022**, *23* (7), 3971.
(117) Paula, S.; Deamer, D. W. Chapter 4 Membrane Permeability Barriers to Ionic and Polar Solutes. In *Membrane Permeability - 100 Years since Ernest Overton*; Deamer, D. W., Kleinzeller, A., Fambrough, D. M., Eds.; Academic Press, 1999; Vol. *48*, pp 77−95. Eds.; Current Topics in Membranes, Vol.
(118) Winter, N. D.; Schatz, G. C. Coarse-Grained Molecular Dynamics Study of Permeability Enhancement in Dppc Bilayers by Incorporation of Lysolipid. *J. Phys. Chem. B* **2010**, *114* (15), 5053−5060.
(119) Venable, R. M.; Krämer, A.; Pastor, R. W. Molecular Dynamics Simulations of Membrane Permeability. *Chem. Rev.* **2019**, *119* (9), 5954−5997.
(120) Issack, B. B.; Peslherbe, G. H. Effects of Cholesterol on the Thermodynamics and Kinetics of Passive Transport of Water through Lipid Membranes. *J. Phys. Chem. B* **2015**, *119* (29), 9391−9400.
(121) Krämer, A.; Ghysels, A.; Wang, E.; Venable, R. M.; Klauda, J. B.; Brooks, B. R.; Pastor, R. W. Membrane Permeability of Small Molecules from Unbiased Molecular Dynamics Simulations. *J. Chem. Phys.* **2020**, *153* (12), 124107.

https://doi.org/10.1021/acsomega.5c07901
ACS Omega 2026, 11, 23728−23742